New approach to measurement of the L_2-L_3 Coster-Kronig transition probability in heavy atoms

J. L. Campbell, P. L. McGhee, R. R. Gingerich, R. W. Ollerhead, and J. A. Maxwell

Guelph-Waterloo Program for Graduate Work in Physics, University of Guelph, Guelph, Ontario, Canada N1G 2W1

(Received 23 January 1984)

The Coster-Kronig probability f_{23} for lead has been measured by a K-x-ray—L-x-ray coincidence technique. Analytic fitting of the $K\alpha$-x-ray triplet using nonlinear least-squares methodology was employed to determine the corrections necessitated by the overlap of the $K\alpha_2$ and $K\alpha_1$ peaks. The result, 0.112 ± 0.002, is to be compared with the Dirac-Hartree-Slater prediction of 0.122 and a recently measured value of 0.130 ± 0.002 obtained by a different approach to the overlap correction. The present result may provide an estimate of relaxation and many-body effects, which—if included—would lower the Dirac-Hartree-Slater single-particle-model prediction.

I. INTRODUCTION

A significant portion of the widths of atomic $L_{1,2}$-subshell vacancy states is due to Coster-Kronig transitions, which promote the vacancy to a higher subshell (L_1-L_2, L_1-L_3, L_2-L_3) prior to L-shell deexcitation by LY x ray or LYZ Auger emission ($Y,Z = M,N,O,\ldots$); they are[1] predominantly nonradiative transitions involving the two L subshells and the outer electron to which the L-subshell energy difference is transferred. During the 1970s a large number of experimental measurements of L_2-L_3 Coster-Kronig transition probabilities (f_{23}) were performed by a K-x-ray—L-x-ray coincidence technique using semiconductor x-ray spectrometers.[2] A much smaller body of data has been accumulated on the L_1-L_2 and L_1-L_3 cases, by methods that were less direct and generally had to assume values for other atomic quantities. In the medium-to-high atomic-number region, f_{23} lies in the range 0.1—0.25 and the uncertainty quoted in most Kx-Lx measurements is $(5—10)\%$. However, the scatter of results[2-5] is markedly greater, as illustrated in the case of lead by Table I. A critical selection[2] of "best" values indicated a general agreement with calculations based on nonrelativistic hydrogenic[6] and Herman-Skillman[7] wave functions.

Any addition to the plethora of experimental data on f_{23} requires justification both as regards any perceived need for improved data and also in terms of significant change or improvement in experimental methodology. There are essentially three motivating factors. The first is the current energetic activity in the area of K,L,M ionization cross sections due to protons and other light ions;[8] in the L-subshell case imprecise knowledge of L-subshell fluorescence and Coster-Kronig probabilities is a limiting factor upon experimental accuracy and hence upon tests of cross-section theory. There is also the related need for an accurate data base[9] for the rapidly emerging elemental analysis technique of proton-induced x-ray emission. Finally there has recently appeared the first comprehensive calculation of L-subshell quantities using the Dirac-Hartree-Slater (DHS) model,[10] which merits precise testing.

The fluctuations in measured f_{23} values (Table I) reflect the progressive recognition and elimination of systematic errors, some of them rather subtle, in the Kx-Lx coincidence technique.[2] The major remaining source of uncertainty in this technique lies in the understanding of the K-x-ray spectra of heavy atoms as observed with a Ge spectrometer. The methodology applied in this paper differs from that of previous f_{23} work and is a derivative of our recent studies of the $K\alpha$- and $K\beta$-x-ray series.[11,12]

II. K-x-RAY—L-x-RAY COINCIDENCE TECHNIQUE

The basic technique, shown schematically in Fig. 1, employs two high-resolution x-ray detectors and a radionuclide source of x rays. Detector 1 is set to record the K- and detector 2 the L-x-ray spectra, respectively. In the simplest case of electron capture involving only nuclear ground states, all true Kx-Lx coincidence events arise

TABLE I. Literature values of the L_2-L_3 Coster-Kronig probability in lead.

	f_{23}
Experimental values	0.164 ± 0.016[a]
	0.156 ± 0.011[b]
	0.105 ± 0.011[c]
	0.121 ± 0.012[d]
	0.130 ± 0.002[e]
Calculated values	0.105[f]
	0.104[g]
	0.122[h]
Present experimental value	0.112 ± 0.002

[a]Reference 3.
[b]Reference 4.
[c]Reference 2.
[d]Revision of Ref. 2 in Ref. 5.
[e]Reference 5.
[f]Reference 6.
[g]Reference 7.
[h]Reference 10.
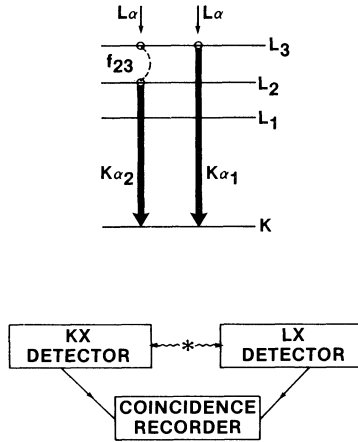
FIG. 1. Schematic diagram of the Kx-Lx coincidence method.

FIG. 2. Pulse-height spectrum from Ge detector due to 66.7-keV γ ray.

from the sequence K capture followed by $K\alpha$-x-ray emission, and subsequent filling of the resulting L vacancy by $M,N,O,\ldots$ electrons, i.e., L-x-ray emission. (Higher-order processes—e.g., shakeoff—may be neglected.) In the L-x-ray spectrum the $L\alpha$ (i.e., L_3M_{45}) peak contains only L_3 x rays and thus signals the filling of L_3 vacancies only. The numbers of $L\alpha$ x rays recorded in coincidence with gates set on the $K\alpha_2$ (signaling an initial L_2 vacancy) and $K\alpha_1$ (signaling an initial L_3 vacancy) peaks are

$$C_{L\alpha}(K\alpha_2) = n(K\alpha_2)f_{23}\omega_3 k(L\alpha)\epsilon(L\alpha) , \tag{1}$$

$$C_{L\alpha}(K\alpha_1) = n(K\alpha_1)\omega_3 k(L\alpha)\epsilon(L\alpha)(1+Q_2A_{22}) , \tag{2}$$

where k is the $L\alpha$ fraction in the L_3-x-ray series, ϵ the absolute detection efficiency, n the number of gating signals, A_{22} an angular correlation coefficient, and Q_2 its geometric attenuation factor. In this simple decay scheme, no true coincidences can occur between L and $K\beta$ x rays since the latter create only $M,N,O,\ldots$ vacancies; f_{23} can be obtained from Eqs. (1) and (2) as

$$f_{23} = \frac{C_{L\alpha}(K\alpha_2)}{C_{L\alpha}(K\alpha_1)} \frac{n(K\alpha_1)}{n(K\alpha_2)} \tag{3}$$

if the angle between the detectors is set at 125° to eliminate the $K\alpha_1$x-$L\alpha$x angular correlation, so that $A_{22}=0$.

With more complex decay schemes involving cascades of electron-capture and internal-conversion processes, true but "spurious" coincidences can occur, e.g., between a K x ray from K capture and an L x ray from a subsequent internal-conversion process in the same atom. McGeorge et al.[13] showed that this contribution could be measured elegantly by recording the L x rays in coincidence with the $K\beta$ line; this approach also corrects for x rays generated by absorption effects in sources that are not ideally "thin."

In this determination of f_{23}, geometric and efficiency factors cancel, and after cascading effects have been taken into account, the principal source of error becomes the purity of the $K\alpha_1$ and $K\alpha_2$ gating signals. As illustrated by Fig. 2, recorded with our Ge spectrometer using a 66.7-keV γ ray, every spectral peak generates a low-energy tail; therefore the low-energy partner ($K\alpha_2$) of the $K\alpha$
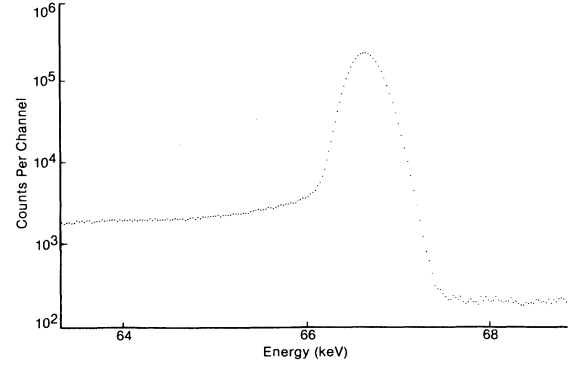
doublet contains a contribution from the high-energy partner ($K\alpha_1$). The number of pure $K\alpha_2$ events accompanied by $L\alpha$ x rays is proportional to $f_{23}\omega_3$, whereas the corresponding number due to the $K\alpha_1$ tail component is proportional to ω_3. If the tail contributes $t\%$ of the $K\alpha_2$ gate, it will increase the $K\alpha_2$-$L\alpha$ coincidence rate by $t\%/f_{23} \simeq 10t\%$. Thus even small tailing contributions can cause significant (and erroneous) increases in measured f_{23} values.

In early measurements of f_{23}, detectors of rather poor tailing characteristics were used and a simple graphical approach was used to estimate the tails. In later work[2] γ rays of similar energy were used to model the $K\alpha_1$ line and determine its contribution to $K\alpha_2$. Although a better approximation, this method ignores the fact that K-x-ray line shapes are essentially Voigt functions,[14] i.e., convolutions of the intrinsic Lorentzian line shape with the quasi-Gaussian detector resolution, whereas γ-ray line shapes give only the resolution function; this approach therefore underestimates the low-energy tailing of the $K\alpha_1$ peak. In quite recent work, Gnade et al.[15] took a new iterative approach to determining the $K\alpha_1$ tail contribution to the $K\alpha_2$ signal, which demands only that the $K\alpha_2$ and $K\alpha_1$ peaks have the same shape and time structure (see Sec. VII).

Even if the low-energy tailing problem can be accurately treated, there remain experimental problems. Most previous experiments used single-channel analyzers to set windows on the $K\alpha_2$ and $K\alpha_1$ peaks. In the absence of digital stabilization, the peak centroids could drift during long runs; also, the analog window settings could drift. Our experimental approach is designed to eliminate these two error sources and to take a more rigorous approach to ascertaining the precise content of the $K\alpha_2$ and $K\alpha_1$ energy windows.

III. EXPERIMENT

The radionuclide chosen for study was [207]Bi, because of the extensive earlier work on this case (Table I). Its decay scheme, shown in Fig. 3, results in cascade contributions to the Kx-Lx coincidence rate. A source of about 1.2 μCi was made by evaporating a drop of bismuth chloride solution to dryness on a 0.05-mm-thick beryllium foil; insulin was added to improve the uniformity. The K-x-ray spectrum was recorded using an Aptec intrinsic germanium
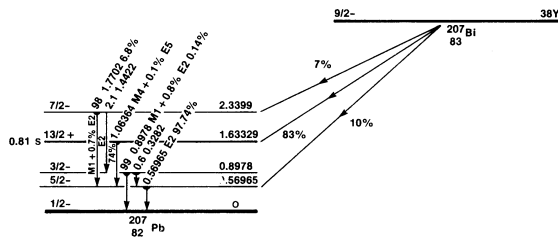
FIG. 3. Decay scheme of ^{207}Bi.

detector of area 80 mm^2, thickness 10 mm, and energy resolution 480 eV at 122 keV. The L x rays were recorded with a Kevex Si(Li) detector of area 80 mm^2 and thickness 3 mm; its resolution was about 180 eV at 5.9 keV. The detectors were placed at an angle of 125° to eliminate the angular correlation between $K\alpha_1$ and L x rays.

Figure 4 is a schematic diagram of the pulse-processing and data-recording system. Its central feature is a Nuclear Data 66 pulse-height analyzer used in "list mode;" when gated by a logic signal indicating that a Kx-Lx coincidence has occurred and that certain other conditions (see below) are satisfied, it records the event in three consecutive analyzer channels. The first channel contains the digitized L-x-ray pulse height, the second the delay time between the two coincident photons measured with a time-to-amplitude converter (TAC), and the third the K-x-ray pulse height; the three analog-to-digital converters (ADC's) have conversion gains of 1024, 1024, and 4096, respectively. The logic signal that initiates recording of an event is generated if the TAC gives an output within a given voltage range and if the K-x-ray pulse-inspection circuitry indicates that the pulse is acceptable on grounds of both rise time and pileup; the logic is vetoed during resets of the Si(Li) pulsed optical circuit. The pileup inspector is internal to the Ortec 572 amplifier. The rise-time inspector consists of two constant fraction discriminators, firing at 20 and 80%, which feed, respectively, the start and stop inputs of a time-to-amplitude converter. The TAC's output is fed to a single-channel analyzer (SCA) set to accept only the peak in the rise-time distribution and to reject the larger pulses corresponding to long rise times. The SCA output thus indicates the presence of
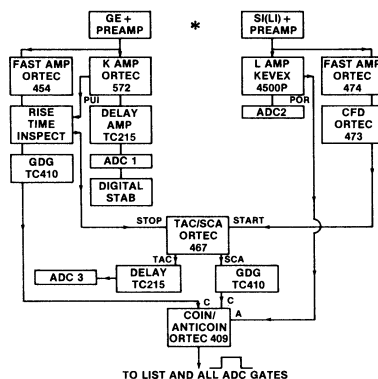
a normal pulse whose rise time has not been slowed by detector imperfections. When one half of the Nuclear Data ND66's 16 384 channels are filled, accumulation transfers to the other half, and the first 8 192 channels are written to disk by a Digital Equipment Corporation Minc-11/23 microcomputer supervising the ND66 analyzer.

The Nuclear Data GEN2 ADC recording the K-x-ray spectra is digitally stabilized. This is generally not feasible in coincidence experiments, since only a very small fraction of the pulses presented to the ADC are accepted, digitized, and fed to the stabilizer. In this case, out of a K-x-ray singles rate of about 1000 per sec, only about 3 per sec were coincidence events, a rate inadequate to provide precise stabilization. An "ADC buffer and stabilizer interface" module was therefore constructed to alter the normal interaction between the ND66 analyzer and the ND LIST module. When there is no accompanying logic pulse the ADC converts the K-x-ray pulse, but the "ready" signal is not permitted to reach the data handler. However, the new buffer device receives the ready signal and generates an address transfer to the stabilizer; the buffer then sends a "clear" signal to the ADC. When a coincident gating pulse accompanies the K-x-ray pulse, the ready signal is transmitted to the data handler and the address is transferred to memory; the data handler then clears the ADC. Hence the stabilizer operates at the singles rate, whereas only coincidence events are presented to the analyzer.

This is an important aspect of our method. It ensures that the $K\alpha_1$ and $K\alpha_2$ peak centroids remain fixed to within ≤ 1 eV. Energy windows are then defined for these peaks by software during playback of the event list from disk and, hence, no experimental errors are introduced by unstable analog windows.

Two separate experiments were conducted, in the first of which no collimation was employed. In the second, a 2.5-mm-thick tin collimator with a 5-mm-diameter circular aperture was interposed between the ^{207}Bi source and the Ge detector. This did not mask any part of the detector but eliminated spectral events arising from photons that had scattered in the aluminum endcap. Each experiment comprised measurement of the stabilized K-x-ray singles spectrum to a high statistical precision and the recording of a list of coincidence events to disk. It should be noted that since Eq. (3) involves only ratios of L-x-ray coincidence spectra and K-x-ray singles intensities, it is acceptable to measure the ratios at different times.

A series of auxiliary measurements was performed to test the analytic function used here to represent the $K\alpha$-x-ray spectrum. These were singles spectrum measurements of Ge spectra for monoenergetic γ rays in the energy region 59—122 keV. The radionuclide sources used were ^{241}Am, ^{153}Gd, ^{170}Tm, ^{171}Tm, and ^{57}Co; the recorded intensity was typically about 3×10^6 counts.

FIG. 4. Electronic arrangement for list recording of coincidence data.

IV. ANALYSIS OF SINGLES DATA

The six γ-ray peaks recorded using the uncollimated Ge spectrometer were fitted by the nonlinear least-squares technique using the expression[14,16]

$$F(x)=G(x)+S(x)+D(x)+B(x) , \qquad (4)$$

where

$$G(x)=H_G\exp[-(x-x_0)^2/2\sigma^2] ,$$

$$S(x)=\tfrac{1}{2}H_S\left[1-\mathrm{erf}\left[\frac{x_0-x}{\sigma\sqrt{2}}\right]\right] ,$$

$$D(x)=\tfrac{1}{2}H_D\exp\left[\frac{x-x_0}{\beta}\right]\mathrm{erfc}\left[\frac{x-x_0}{\sigma\sqrt{2}}+\frac{\sigma}{\beta\sqrt{2}}\right] ,$$

$$B(x)=a+bx .$$

In this expression, $G(x)$ is the Gaussian line shape expected from a perfect detector; the complementary error function $S(x)$ models the low-energy step; and the function $D(x)$, an exponential convoluted with a unit-area Gaussian, models the low-energy tail. The linear function $B(x)$ models the underlying continuum arising from higher-energy events.

Campbell and Jorch[16] demonstrated the success in the Ge(Li) case of a similar function with two tails $D_L(x)$ and $D_S(x)$ representing different degradation processes. With the present Ge detector, only one tail $D(x)$ was needed to achieve good fits to spectra containing $\sim 3\times10^6$ counts, as indicated by the reduced chi-squared values in Table II. The area of the tailing function $D(x)$ as a fraction of the Gaussian area was essentially constant (3.7%) across the 60–120-keV energy range of interest. The addition of a second tailing function had a variable outcome, sometimes improving the goodness of fit slightly and sometimes having little effect; generally, the second tail had such a shallow slope that it was scarcely distinguishable from the step function $S(x)$ in shape. With the collimator present, the height of the step function fell by about 30% but the area of the single tail $D(x)$ remained at the 3.5% value; the quality of fits remained very good.

The $K\alpha$-x-ray spectrum of lead contains three peaks, one of which, the *l*-forbidden L_1-K line, is very weak and is obscured in the data of Fig. 5 by the $K\alpha_2$ peak. Nevertheless, it was included in the fitting procedure. Since the parameters of the step and tail functions are observed in the γ-ray case to vary little in relation to the Gaussian parameters over the energy region spanned by the lead K x rays, it was not necessary to triple their num-

ber. Instead, the ratios $P_1=H_S/H_G$, $P_2=H_D/H_G$, and $P_3=\beta/\sigma$ were taken to be the same for each x-ray line, so that the number of distortion parameters was not increased over the γ-ray case. To maintain linear channel-energy calibration, together with the correct energy dependence of peak width, the x_0 and σ values were described by

$$x_0=P_4+P_5E ,$$
$$\sigma^2=P_5+P_6E , \qquad (5)$$

adding four parameters. With 2 background parameters and 3 Gaussian heights we reach 12 parameters for the $K\alpha$ triplet. However, as indicated earlier, each K-x-ray peak is the convolute of the detector response function with the intrinsic Lorentzian line profile

$$L(x)=\frac{\Gamma/2\pi}{(x-x_0)^2+(\Gamma/2\pi)^2} . \qquad (6)$$

Hence a 13th parameter Γ is added, and the fitting function is

$$F(x)=B(x)+\sum_{i=1}^{3}L_i(x)^*[G_i(x)+S_i(x)+D_i(x)] , \qquad (7)$$

where the asterisk denotes numerical convolution. In earlier work[14] we used a Voigt function approximation to L^*G but here all components of the resolution function are convoluted using a numerical technique.

The results of fitting the lead $K\alpha$-x-ray spectra are in Table III. In experiment I, with no collimator on the Ge detector, Eq. (7) gave a good fit with $\chi_r^2=1.5$; addition of a second tail function (bringing the number of parameters to 15) improved the value of χ_r^2 but did not significantly alter the contents of the two windows set to span the full width at one-tenth maximum of the $K\alpha_2$ and $K\alpha_1$ peaks. In the second experiment, with the collimator in place, the fit was slightly poorer. Table III also includes values of the intensity-independent quantity

$$(\overline{\Delta^2})^{1/2}=d(\chi_r^2-1)/I \qquad (8)$$

(where d represents the number of degrees of freedom and I represents the total counts) developed by Sekine and Baba.[17] This is the root mean square of the deviations between the model [Eq. (7)] and the true distribution; its low value again attests to the high quality of the fits.

Due to the decreased low-energy step intensity in the collimated experiment, it was possible to observe visually a very weak bismuth $K\alpha_1$-x-ray line on the upper side of the lead $K\alpha_1$ line; this implies the presence of the corresponding $K\alpha_2$ line between the lead $K\alpha_2$ and $K\alpha_1$ lines. These contributions arise from naturally occurring radionuclides in the cryostat; although they worsen the fit slightly, their effect on the final f_{23} value is negligible.

Five windows were set on the K-x-ray spectrum; some of those for experiment I are shown in Fig. 5. They span the $K\alpha_2$ and $K\alpha_1$ peaks, the $K\beta$ group, and continuum regions just above $K\alpha$ and $K\beta$. In the notation adopted here for the contributions to these windows, the bracketed quantity is the window setting ($K\alpha_2$, $K\alpha_1$, $A\alpha$, $K\beta$, $A\beta$) and the superscript denotes the particular contribution to

TABLE II. Details of fits of Eq. (4) to γ-ray peaks.

Energy (keV)	Width of region fitted (keV)	Number of counts	χ_r^2
59.54	6.10	3.18×10^6	1.56
66.7	4.72	3.08×10^6	1.17
66.7[a]	4.72	2.32×10^6	1.23
84.26	6.05	3.93×10^6	1.03
97.43	6.03	4.61×10^6	1.52
103.18	7.45	3.03×10^6	1.17
103.18[a]	7.45	1.52×10^6	1.01
122.1	8.0	3.39×10^6	1.89

[a]In these cases a tin collimator of 5 mm aperture was present.
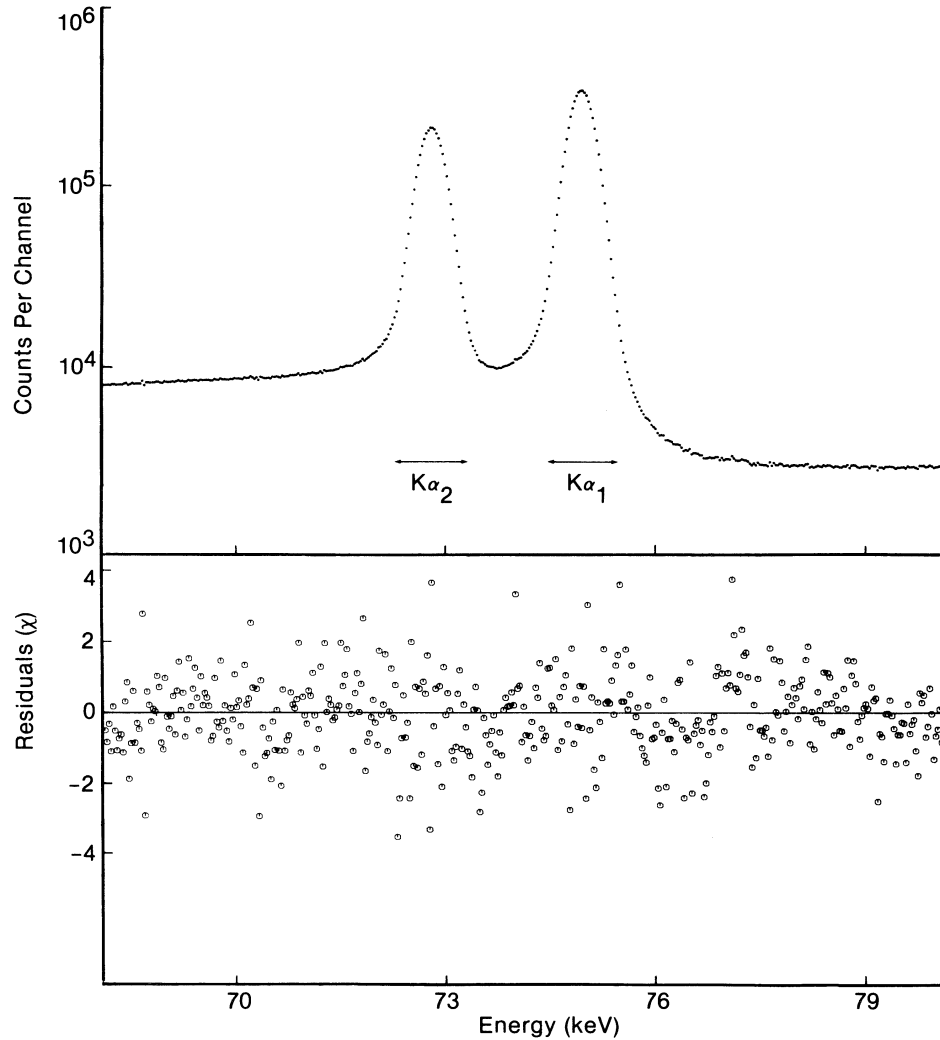
FIG. 5. Measured pulse-height spectrum of the lead $K\alpha$-x-ray series and residuals from fit to Eq. (7). Residuals are in units of one standard deviation.

that window. Thus $n^{K\alpha_1}(K\alpha_2)$ is the number of $K\alpha_1$ counts within the energy window set on the $K\alpha_2$ peak, and $n^{A\alpha}(K\alpha_2)$ is the background continuum intensity in that window. The data for the $K\alpha_2$ and $K\alpha_1$ windows were of course deduced from the fitted $K\alpha$ multiplet. The data for the other three windows were taken directly from the experimental singles spectrum. The last column of Table III shows the critical quantity $n^{K\alpha_1}(K\alpha_2)/n^{K\alpha_2}(K\alpha_2)$, i.e., the degree of $K\alpha_1$ tailing into the $K\alpha_2$ window. In experiment II, narrower $K\alpha_1$ and

$K\alpha_2$ windows were defined, approximately equal to the full width at half maximum of the peaks. This redefinition, together with the reduction in tailing afforded by collimation, afforded a reduction of almost a factor of 2 in the ratio $n^{K\alpha_1}(K\alpha_2)/n^{K\alpha_2}(K\alpha_2)$.

V. ANALYSIS OF COINCIDENCE DATA

The time distribution of all Kx-Lx coincidences was reconstructed from the event list using software written

TABLE III. Results of fits of Eq. (7) to the lead $K\alpha$ spectrum.

Measurement	Number of counts	χ_r^2	$(\Delta^2)^{1/2}$	Γ (eV)	$K\alpha_3/K\alpha_1$	$\dfrac{n^{K\alpha_1}(K\alpha_2)}{n^{K\alpha_2}(K\alpha_2)}$
Expt. I, 1 tail fit	1.30×10^7	1.50	1.6×10^{-5}	74.0	1.18×10^{-3}	4.43%
Expt. I, 2 tail fit	1.30×10^7	1.21	0.65×10^{-5}	73.1	0.9×10^{-3}	4.44%
Expt. II, 2 tail fit	2.37×10^7	2.42	2.3×10^{-5}	72.3	0.95×10^{-3}	2.30%

for the Digital Equipment Corporation RT-11 operating system. Energy windows were set on the energy regions 69.5—107.0 keV in the Ge spectrum and 3—19 keV in the Si(Li) spectrum. The resulting spectrum from ADC2 (TAC) is shown in Fig. 6.

The principal reconstruction, viz., that of the coincident L-x-ray spectrum from ADC1, was then performed, with windows set on the events of ADC2 and ADC3 as follows. Two windows were set on the time data from ADC2 as shown in Fig. 6. The central window included real and random coincidence events; the composite of two "half-windows" set on the continuum included essentially random events only. Five windows were defined for the K-x-ray data from ADC3, as indicated in Fig. 5 and the preceding section. The software then generated ten x-ray spectra, the first five including real plus random coincidences for the five K-x-ray regions and the second five the corresponding random coincidences. From each of the first five spectra, the random coincidence partner was subtracted to produce the true L-x-ray spectra coincident with the five different types of K-x-ray events. These are denoted $S_{Lx}^0(K\alpha_2)$, $S_{Lx}^0(K\alpha_1)$, $S_{Lx}^0(A\alpha)$, $S_{Lx}^0(K\beta)$, $S_{Lx}^0(A\beta)$. The superscript zero signifies that no corrections have been made.

A series of subtractive corrections was now made to these spectra to remove contributions from other than the desired direct Kx-Lx coincidences arising from (M,N,O)-L-K atomic cascades. The superscript zero simply denotes that no corrections have yet been effected. Note that the manipulations are carried out upon the entire spectra, not on any particular peak intensity, and that superscripts 1,2,3 represent stages of correction.

The L-x-ray spectrum coincident with the $K\alpha_1$ window contains a contribution from the $n^{A\alpha}(K\alpha_1)$ continuum events in that window; this was removed by subtracting the normalized $S_{Lx}^0(A\alpha)$ spectrum, viz.,

$$S_{Lx}^1(K\alpha_1)=S_{Lx}^0(K\alpha_1)-\frac{n^{A\alpha}(K\alpha_1)S_{Lx}^0(A\alpha)}{n^{A\alpha}(A\alpha)} . \qquad (9)$$

A similar correction was made to obtain $S_{Lx}^1(K\alpha_2)$. In obtaining $S_{Lx}^1(K\beta)$, the region above $K\beta$ in the K spectrum was fitted to a straight line, which was extrapolated back under the $K\beta$ peak.

The spectra $S_{Lx}^1(K\alpha_1)$ and $S_{Lx}^1(K\alpha_2)$ after this continuum correction contain two types of real coincidence. The first (A) is the desired type, i.e., a Kx-Lx cascade filling a K vacancy in a single atom. In the second type (B), a K x ray is detected in the Ge spectrometer but the subsequent L x ray is not observed by the Si(Li); instead a second process, e.g., internal conversion, occurs in that atom and the Si(Li) detects the resulting L x ray. McGeorge *et al.*[13] first pointed out that since $K_\beta x$-Lx coincidences could only arise from the second process ($K\beta$ emission does not result in an L vacancy), such coincidences would provide a precise measure of the contribution of this process. Thus

$$S_{Lx}^2(K\alpha_1)=S_{Lx}^1(K\alpha_1)-\frac{n^{K\alpha}(K\alpha_1)}{n^{K\beta}(K\beta)}S_{Lx}^1(K\beta) \qquad (10)$$

and similarly for $S_{Lx}^2(K\alpha_2)$.

The final correction adjusts for the overlap of the $K\alpha_2$ and $K\alpha_1$ line shapes (mainly via the D and S components of $K\alpha_1$ underlying $K\alpha_2$) in the singles K-x-ray spectrum. An iterative procedure was used. At the outset the $K\alpha_1$ window (the "purer" of the two) was assumed to contain no $K\alpha_2$ counts, so that a first approximation to $S_{Lx}^3(K\alpha_2)$ could be obtained via

$$S_{Lx}^3(K\alpha_2)\approx S_{Lx}^2(K\alpha_2)-\frac{n^{K\alpha_1}(K\alpha_2)}{n^{K\alpha_1}(K\alpha_1)}S_{Lx}^2(K\alpha_1) , \qquad (11)$$

where the ratio of "n" values was obtained from the pre-
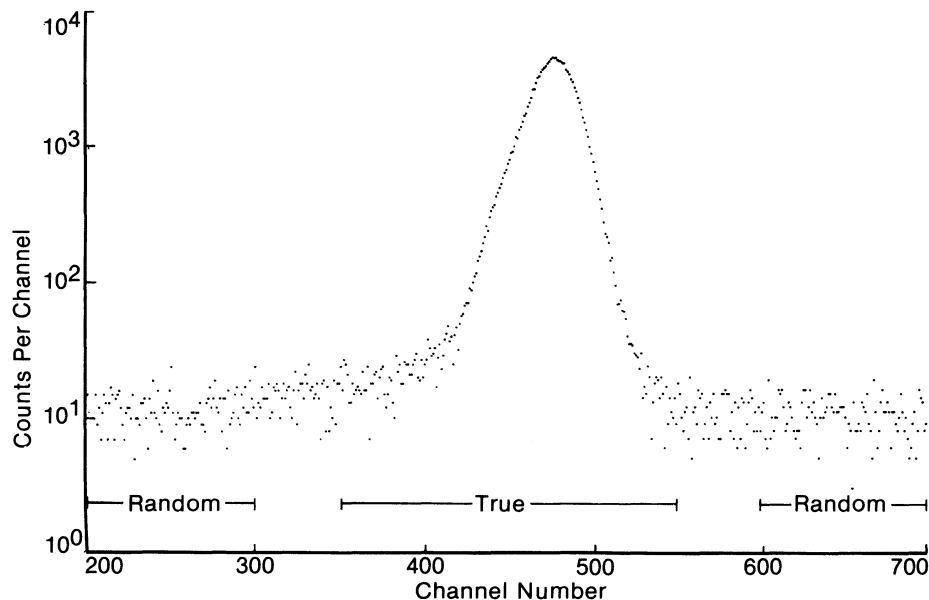
FIG. 6. Time distribution of Kx-Lx coincidences.

viously described fitting procedure. The process was reversed, viz.,

$$S_{Lx}^3(K\alpha_1)=S_{Lx}^2(K\alpha_1)-\frac{n^{K\alpha_2}(K\alpha_1)}{n^{K\alpha_2}(K\alpha_2)}S_{Lx}^3(K\alpha_2) , \qquad (12)$$

and the result of this step substituted back in place of $S_{Lx}^2(K\alpha_1)$ in Eq. (11). These three iterations were sufficient to achieve consistency.

Table IV gives the $L\alpha$-x-ray intensities at each stage of this process and thus indicates the relative importance of the corrections. The first (continuum) correction is very small, compared to the corrections for cascade processes and $K\alpha_2$-$K\alpha_1$ peak overlap. These numbers reinforce our earlier comment that the $K\alpha_2$-$K\alpha_1$ overlap is the critical factor. The contribution to $C_{L\alpha}(K\alpha_2)$ from coincidences with the $K\alpha_1$ tail in experiment I is 25.8% of all recorded $L\alpha$ x rays coincident with the $K\alpha_2$ gate or 39.8% when expressed as a fraction of the final corrected intensity. The latter figure corresponds closely to the quantity t/f_{23}

TABLE IV. $L\alpha$-x-ray intensities.

	Experiment I		Experiment II	
	$C_{L\alpha}(K\alpha_2)$	$C_{L\alpha}(K\alpha_1)$	$C_{L\alpha}(K\alpha_2)$	$C_{L\alpha}(K\alpha_1)$
Raw	13 925	138 075	11 172	126 529
S_{Lx}^1	13 751	137 914	11 092	126 431
S_{Lx}^2	12 617	136 297	10 272	125 061
S_{Lx}^3	9 024	135 984	8 500	125 053

calculated from the $t=n^{K\alpha_1}(K\alpha_2)/n^{K\alpha_2}(K\alpha_2)$ of Table III and our final f_{23} value. In experiment II, where collimation decreased tailing and a narrower energy window was used, this contribution was 15.9% of all recorded $L\alpha$ x rays coincident with $K\alpha_2$ or 20.8% of the final corrected intensity.

Figure 7 shows the final L-x-ray spectra from experiment II. All of the tabulated $L\alpha$ line intensities were obtained by simple linear interpolation of background under
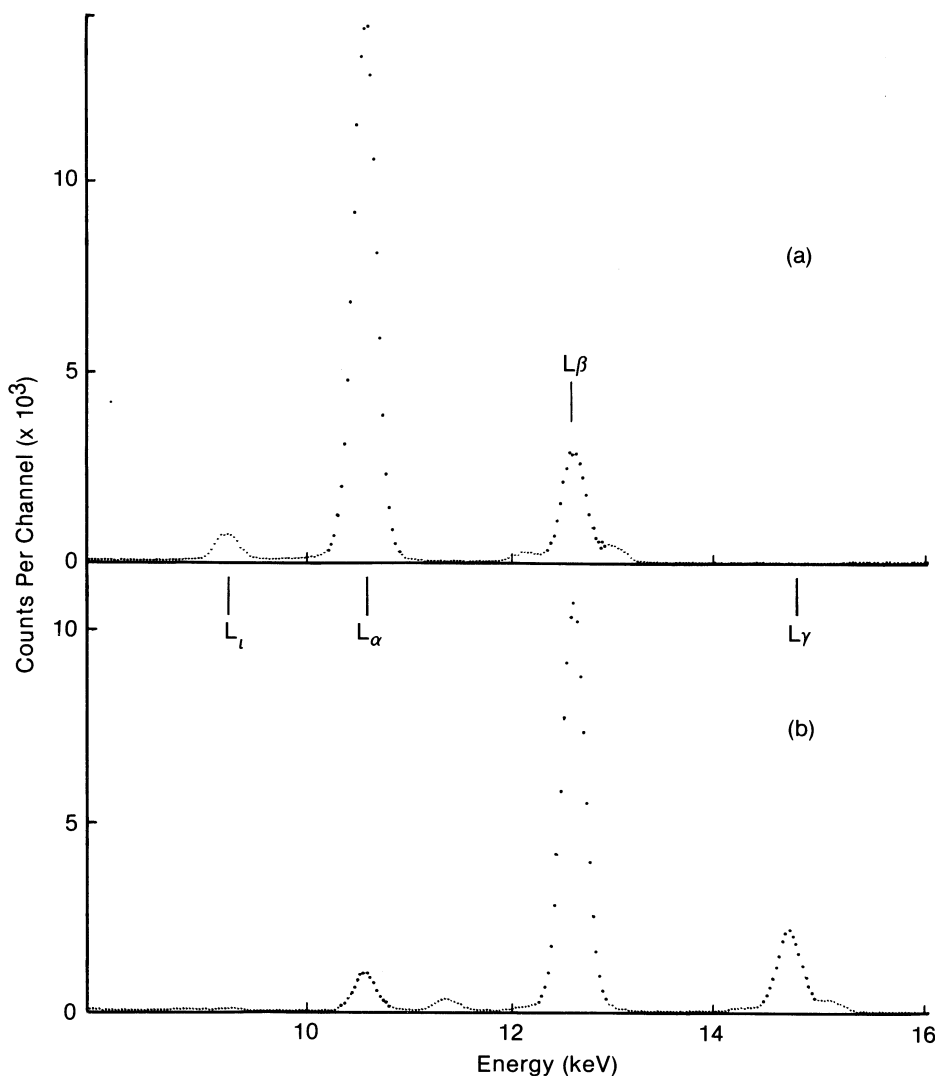
FIG. 7. Final coincident L-x-ray spectra in experiment II (i.e., after all corrections described in Sec. V): (a) is in coincidence with $K\alpha_1$ x rays and (b) with $K\alpha_2$ x rays.

the peak. However, nonlinear least-squares fits to the Ll-$L\alpha$-$L\eta$ region were also done using Gaussian line shapes.

VI. RESULTS

In calculating f_{23} from the coincident intensities $C_{L\alpha}(K\alpha_1)$ and $C_{L\alpha}(K\alpha_2)$, the means of intensities from the two approaches to the L-x-ray spectrum were used. The f_{23} values from experiments I and II are, respectively, 0.111 and 0.113, each with a statistical error of $\pm 1.5\%$ (one standard deviation).

A consideration of the systematic uncertainty inherent in our analytic fitting of the $K\alpha$ triplet is necessary since this is the crux of the experimental method. The fits to the singles spectra are excellent, given their very high intensity (13×10^6 and 24×10^6 counts, respectively). The Lorentzian linewidths (Γ) are close to the theoretical value[18] of 66.5 eV. Hence, our line shapes are much superior to those deduced by modeling with γ rays. Nevertheless, the fits are not perfect; one reason for this is the presence of KLM and KLN radiative Auger satellites in the $K\alpha$-x-ray region.

The principal source of error in f_{23} is the estimate of the $K\alpha_1$ tail contribution to the $K\alpha_2$ energy window. In experiment I this tail resulted in 3593 $L\alpha$ x rays coincident with the $K\alpha_2$ window, which is a large correction, amounting to 39.8% of the final 9024 true $L\alpha$ events given in Table IV. The single-tail fit to the singles $K\alpha$-x-ray spectrum of experiment I indicated that 97% of the $K\alpha_1$ tail contribution in the $K\alpha_2$ window arose from the step function $S(x)$; this is essentially flat in this region, and the uncertainty in its height and hence in its overall contribution was given as $\pm 0.8\%$ by the appropriate diagonal element of the error matrix. There is thus a $\pm 0.8\%$ uncertainty in the number of $K\alpha_1$ events with the $K\alpha_2$ window. This translates into a $\pm 0.3\%$ uncertainty in the quantity $C_{L\alpha}(K\alpha_2)$ and hence also in f_{23}.

Some further, albeit crude, estimates of uncertainty can be arrived at by examining the results for the $K\alpha_3/K\alpha_1$ relative radiative transition probability. Our mean value for this ratio of the L_1-K magnetic dipole transition rate to the predominant L_3-K electric dipole transition rate is 1.01×10^{-3}, whereas the DHS prediction[19] is 0.97×10^{-3}. If we took the 0.04×10^{-3} discrepancy seriously (it is well within the uncertainties of the fit) and attributed it entirely to an erroneous determination of the $K\alpha_1$ tail intensity, it would imply a 0.33% error in the latter, corresponding to a 0.13% error in f_{23}. This is certainly a worst-case estimate since some of the discrepancy must arise from error in the $K\alpha_2$ intensity.

Our final estimate of the error due to $K\alpha_2$-$K\alpha_1$ overlap is thus under 1%, but we shall adopt a 1% value in order to be conservative. This is added in quadrature with a 1.5% statistical error and a 1% error arising from definition of the $L\alpha$ peak. Thus

$$f_{23} = 0.112 \pm 0.002$$

at a 63% confidence level (1σ equivalent).

VII. DISCUSSION

Previous results for f_{23} in lead have oscillated widely as various systematic errors were eliminated. Because of these recognized errors we have to discount all but the last experimental value of the Atlanta school, quoted in Table I, viz., $f_{23} = 0.130 \pm 0.002$. This is 6% greater than the DHS prediction of Chen *et al.*,[10] viz., 0.122. In contrast, our value of 0.112 ± 0.003 is some 9% lower. The 15% difference attests to the great difficulty of estimating the tailing of the $K\alpha_1$ member of the $K\alpha$-x-ray doublet.

Our result includes a crude estimate of the error (at 1σ level) introduced by our approach to estimating this tailing. The definition of the error in Ref. 5 is not clear, but it is likely to be entirely statistical. It is tempting to conclude that we and Tan *et al.*[5] have both underestimated systematic errors and, by taking the mean of both our results, to conclude that very strong support for the theory emerges. However, we have reasons to stand by the lower value obtained here. First, all earlier work has used γ-ray peaks to model the $K\alpha_1$-x-ray line shape. It is straightforward to calculate that for our particular detector that approach would have generated a 5% *over*estimate of f_{23}. Second, one reason that the older results of the Atlanta group have been revised upwards is their recent observation[15] of the following subtlety. In the singles K-x-ray spectrum a certain degree of $K\alpha_1$ tailing under the $K\alpha_2$ peak is observed. However, in the recording of Kx-Lx coincidences, the necessary imposition of a reasonably short resolving time eliminates those K-x-ray pulses having slow rise times; since these lie mainly in the low-energy tail, the effective tailing is less than would have been calculated from the singles. Prior downward corrections of f_{23} to account for the tailing were decreased upon recognition (and an elegant demonstration) of this effect,[15] leaving a group of f_{23} values[5] at high Z that generally exceed DHS theory.[10] Our experimental method removes such pulses by rise-time inspection prior to the registration of a coincidence event and so this rather complex problem of assessing the altered tail contributions in coincidence mode does not arise.

There are very few measurements of f_{23} at high Z (and below the discontinuities in $91 \le Z \le 94$) by techniques other than the Kx-Lx method. However, at $Z = 88$ there exists a measurement[20] by an L-conversion-electron—L-x-ray coincidence technique which is free of the peak overlap problems discussed above. This result lies 7% below the DHS prediction.

We conclude that there is a strong indication from experiment that the DHS calculations overestimate the L_2-L_3 Coster-Kronig transition probability at high Z by some $(5-10)\%$. Such an overestimate is to be expected since various effects omitted in single-particle calculations all tend, when included, to reduce Coster-Kronig transition rates. These effects include configuration interaction and relaxation, and the exchange of the emitted electron with bound electrons. They have not been studied for the L_2 shell, but a recent investigation[21] of them for the particular case of the L_1 shell in argon shows that they are significant. Nevertheless, more experimental results from our approach and from that described by Gnade *et al.*[15]

are needed, and the 15% discrepancy between the two approaches must be resolved before firm conclusions can be reached. In this paper we have felt it necessary to describe our method in detail since this is its first application. We intend to report several measurements in the range $70 \leq Z \leq 95$, refine the technique through an improved Ge detector, and extend it to measure the fluorescence yields ω_2 and ω_3.

ACKNOWLEDGMENTS

[1]M. H. Chen, B. Crasemann, P. V. Rao, J. M. Palms, and R. E. Wood, Phys. Rev. A **4**, 846 (1971).

[2]D. W. Nix and R. W. Fink, Z. Phys. A **273**, 305 (1975).

[3]P. V. Rao, R. E. Wood, J. M. Palms, and R. W. Fink, Phys. Rev. **178**, 1997 (1969).

[4]R. E. Wood, J. M. Palms, and P. V. Rao, Phys. Rev. **187**, 1497 (1972).

[5]M. Tan, R. A. Braga, R. W. Fink, and P. V. Rao, Phys. Scr. **25**, 536 (1982).

[6]M. H. Chen, B. Crasemann, and V. O. Kostroun, Phys. Rev. A **4**, 1 (1971).

[7]E. J. McGuire, Phys. Rev. A **3**, 587 (1971).

[8]H. Paul, Nucl. Instrum. Methods **192**, 11 (1982).

[9]J. L. Campbell, J. A. Cookson, and H. Paul, Nucl. Instrum. Methods **212**, 427 (1983).

[10]M. H. Chen, B. Crasemann, and H. Mark, Phys. Rev. A **24**, 177 (1981).

[11]J. L. Campbell and C. W. Schulte, Phys. Rev. A **22**, 609 (1980).

[12]J. A. Maxwell and J. L. Campbell, Phys. Rev. A **29**, 1174 (1984).

[13]J. C. McGeorge, H. U. Freund, and R. W. Fink, Nucl. Phys. A **154**, 526 (1970).

[14]C. W. Schulte, H. H. Jorch, and J. L. Campbell, Nucl. Instrum. Methods **174**, 549 (1980).

[15]B. E. Gnade, R. A. Braga, W. R. Western, J. L. Wood, and R. W. Fink, Nucl. Instrum. Methods **164**, 163 (1979).

[16]J. L. Campbell and H. H. Jorch, Nucl. Instrum. Methods **159**, 163 (1979).

[17]T. Sekine and H. Baba, Nucl. Instrum. Methods **133**, 171 (1976).

[18]M. O. Krause and J. H. Oliver, J. Phys. Chem. Ref. Data **8**, 329 (1979).

[19]J. H. Scofield, Phys. Rev. A **9**, 1041 (1974).

[20]J. L. Campbell, L. A. McNelles, J. S. Geiger, R. L. Graham, and J. S. Merritt, Can. J. Phys. **52**, 488 (1974).

[21]Kh. R. Karim, M. H. Chen, and B. Crasemann, Phys. Rev. A **28**, 3355 (1983).